

## Velocity and temperature scaling in a rough wall boundary layer

R. A. Antonia and R. J. Smalley

*Department of Mechanical Engineering, University of Newcastle, New South Wales 2308, Australia*

(Received 31 January 2000)

Measurements of the three velocity fluctuations  $u$ ,  $v$ ,  $w$  and of the temperature fluctuation  $\theta$  have been made in a turbulent boundary layer roughened by wall-mounted spanwise cylindrical rods regularly spaced in the streamwise direction. Power-law exponents have been estimated for spectra, cospectra, and the corresponding structure functions associated with  $u$ ,  $v$ ,  $w$ , and  $\theta$  at various locations across the layer. In the scaling range, the  $u$  and  $v$  spectra exhibit the largest and smallest slopes, respectively. The slope of the temperature spectrum is quite close to that of the spectrum corresponding to the mean turbulent energy  $\langle q^2 \rangle$ . The scaling range slope of the  $u\theta$  cospectrum is greater than that of the  $uv$  cospectrum which, in turn, is slightly larger than that of the  $v\theta$  cospectrum. These observations are fully supported by the relative behavior of the structure functions. The magnitudes of the scaling exponents decrease as the wall is approached while those of the intermittency exponents increase.

PACS number(s): 47.27.Nz, 47.27.Lx, 47.27.Gs

### I. INTRODUCTION

It has been pointed out [1,2] that, for turbulent shear flows, the inertial range (IR) slope,  $n_\theta$ , of the scalar spectrum is less steep than anticipated unless the magnitude of the Taylor microscale  $R_\lambda$  Reynolds number exceeds about 1000. This behavior is not unique to the scalar spectrum. Spectra of the lateral velocity fluctuation  $v$  also have an inertial range slope  $n_v$  whose magnitude is typically smaller than that (5/3) predicted by the Kolmogorov 1941 [3], or K41, phenomenology unless  $R_\lambda$  is at least 1000. A plausible explanation for this behavior is that isotropy in the inertial range, a key ingredient of K41, is not strictly satisfied unless  $R_\lambda$  is large, possibly even larger than 10 000. There is evidence [4–6], based primarily on the relative behavior of  $\langle (\delta u)^2 \rangle$  and  $\langle (\delta v)^2 \rangle$ , the second-order longitudinal and transverse velocity structure functions [here  $\delta u \equiv u(x+r) - u(x)$  and  $\delta v \equiv v(x+r) - v(x)$  are the increments of the longitudinal  $u$  and lateral  $v$  velocity fluctuations,  $r$  is the component of the separation vector along the  $x$  direction] to indicate that K41, or more appropriately the refined phenomenology of the Kolmogorov 1962 [7], will be approached asymptotically. There is also evidence [5] suggesting that this approach may not be universal, in that the exponents for  $\langle (\delta v)^2 \rangle$  may vary in different flows, or even in different regions of the same flow, for nominally the same range of  $R_\lambda$ .

There are only a few experiments (e.g., [8]) where measurements of all three velocity fluctuations as well as the scalar fluctuation are available. In [8], the focus was entirely on comparing the turbulent energy spectrum  $\phi_q(k_1)$ , defined such that  $\int_0^\infty \phi_q(k_1) dk_1 = \langle q^2 \rangle \equiv \langle u^2 \rangle + \langle v^2 \rangle + \langle w^2 \rangle$  ( $w$  is the spanwise velocity fluctuation and  $k_1$  is the one-dimensional wave number) or twice the mean turbulent kinetic energy, with the temperature spectrum  $\phi_\theta(k_1)$ , defined such that  $\int_0^\infty \phi_\theta(k_1) dk_1 = \langle \theta^2 \rangle$  ( $\theta$  is the temperature fluctuation). When normalized to unity area, the distribution of  $\phi_\theta(k_1)$  and  $\phi_q(k_1)$ , measured in a number of turbulent shear flows, were found to virtually coincide, at least over a range of  $k_1$  which contributes significantly to the variances  $\langle \theta^2 \rangle$  and  $\langle q^2 \rangle$ . The

previous observations would suggest that the magnitude of  $n_q$ , the IR slope of  $\phi_q(k_1)$ , viz.,  $\phi_q(k_1) \sim k_1^{-n_q}$ , should be close to that of  $n_\theta$ . Alternately, in the context of second-order structure functions, the expectation is that  $\zeta_q$  and  $\zeta_\theta$  should have approximately the same magnitude [9]. Here,  $\zeta_\beta$  represents the IR exponent of  $\langle (\delta\beta)^2 \rangle$ , viz.,  $\langle (\delta\beta)^2 \rangle \sim r^{\zeta_\beta}$ , where, in general,  $\delta\beta \equiv \beta(x+r) - \beta(x)$ . The similarity between  $\langle (\delta q)^2 \rangle$  and  $\langle (\delta\theta)^2 \rangle$  was considered in some detail in [9] for values of  $r$  in the dissipative and inertial ranges as well as when  $r$  is comparable to the integral length scale  $L$ . Reasonable support for  $\zeta_q \approx \zeta_\theta$  has been obtained in the wake of a slightly heated circular cylinder [10]. The boundary layer data of Mestayer [11] at  $y/\delta \approx 0.33$  ( $y$  is the wall normal coordinate and  $\delta$  the boundary layer thickness) suggested that  $n_q \approx n_\theta$ . Sreenivasan [2] has already noted that, for the latter data,  $n_\theta \approx 1.49$ , a value significantly smaller than the Corrsin-Obukhov [12] value of 5/3. While the discrepancy may in part be attributed to an insufficiently large  $R_\lambda$  (= 616 in this case), other factors, such as the wall surface condition and the mean shear, cannot be dismissed. It is important to know how these factors affect the relative magnitudes of  $n_\beta$  or  $\zeta_\beta$ . In the context of a smooth wall turbulent channel flow, the magnitude of  $\zeta_u$  has been found to decrease as the wall is approached, a result ascribed to the intermittent presence of near-wall organized and relatively intense vortical structures [13–15]. This would in turn lead to an increased intermittency of the energy dissipation rate, consistent with the observed departure from  $\zeta_u$  from K41.

In this paper, we consider a boundary layer over a specific type of roughness with the wall slightly heated so that temperature can be treated as a passive scalar. The fluctuations  $(u, v, \theta)$  and  $(u, w, \theta)$  are obtained in separate experiments, as a function of distance from the wall. This allows estimates of both  $n_\beta$  and  $\zeta_\beta$  to be obtained, the latter using two different methods. Special attention is paid to the similarity between  $\phi_q$  and  $\phi_\theta$  or between  $\langle (\delta q)^2 \rangle$  and  $\langle (\delta\theta)^2 \rangle$ . In particular, we consider how  $n_q$  (or  $\zeta_q$ ) and  $n_\theta$  (or  $\zeta_\theta$ ) vary when the surface is approached. An attempt is made to quantify the intermittency associated with different quantities using the scaling range in  $\langle (\delta u)^2 (\delta\beta)^4 \rangle$ .

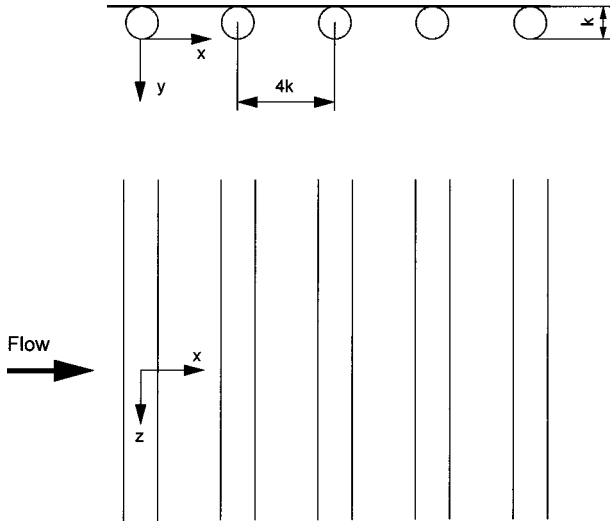


FIG. 1. Rod roughness geometry. Plan and elevation views are shown together with coordinate axes.

## II. EXPERIMENTAL DETAILS

Measurements were carried out in a zero-pressure gradient turbulent boundary layer over a rod-roughened wall. A detailed description of the wind tunnel was given in [16]. The boundary layer was tripped by a 4-mm-diam cylindrical rod followed by a 150-mm-wide strip of No. 40 sandpaper. The roughness extends 3 m downstream of the trip and consists of cylindrical copper rods (Fig. 1) spanning the height of the tunnel [the boundary layer develops over a slightly heated aluminum wall in the  $x$ -vertical ( $x$ - $z$ ) plane]. The rods are placed at a streamwise pitch to roughness height ratio ( $p/k$ ) of 4. The wall temperature,  $T_w$ , was constant over the first 2.5 m of the boundary layer and  $\Delta T$  ( $\equiv T_w - T_1$ , where  $T_1$  is the ambient temperature) was 12.3 °C. To a good approximation, the flow may be considered to be free from buoyancy effects, since at a distance  $x=2.1$  m from the trip,  $Gr_x/Re_x^2$  ( $\equiv [g\beta\Delta T x^3/\nu^2]/[U_1 x/\nu]^2$ )  $\approx 0.002$ ;  $\beta$  is the coefficient of thermal expansion and  $U_1$  is the freestream velocity.

For  $U_1=20$  ms $^{-1}$ , the Reynolds number based on momentum thickness,  $R_\theta$  ( $\equiv U_1\delta_2/\nu$ ;  $\delta_2$  is the momentum thickness), was 15 000. The Reynolds stresses and turbulent heat fluxes were measured using two probes aligned in the  $x$ - $y$  and  $x$ - $z$  planes. Both consisted of a cold wire located immediately upstream and perpendicular to the plane of the X wire. This arrangement minimized the influence of the hot wire on the cold wire. The wires ( $d_w=1.25$   $\mu$ m Pt-10% Rh) of the X probe in the  $x$ - $y$  plane were etched to an active length  $l_w$  of 0.21 mm. The separation between the wires was 0.4 mm and the included angle was 95°. A separate experiment was carried out with an X probe in the  $x$ - $z$  plane. The wires ( $d_w=2.5$   $\mu$ m,  $l_w=0.5$  mm) were separated by 0.45 mm; the included angle was 104°. The cold wire ( $d_w=0.6$   $\mu$ m Pt-10% Rh) for both probes was etched to  $l_w=0.62$  mm. The hot and cold wires were operated by in-house constant temperature (at an overheat ratio of 1.5) and constant current (0.1 mA) anemometers, respectively. The probe was calibrated in the freestream of the working section against a Pitot tube connected to a Furness manometer. The yaw calibration was performed over  $\pm 20^\circ$ . Each probe was

TABLE I. Kolmogorov scales and flow parameters  $R_\lambda$  and  $S^*$ .

$y/\delta$	$R_\lambda$	$\eta$ (mm)	$u_K$ (ms $^{-1}$ )	$S^*$
0.09	280	0.054	0.28	0.052
0.19	330	0.060	0.26	0.057
0.37	390	0.067	0.23	0.053

traversed in the  $y$  direction. A typical record duration was 32 s although longer durations (200 s) were used at five  $y$  locations. The signals were low-pass filtered (cutoff frequency  $f_c=16$  kHz), using fourth-order Butterworth filters and digitized at a frequency  $f_s=2f_c$  with a 12-bit sample-and-hold A-D converter. The choice of  $f_c$  was estimated from the spectra of the unfiltered differentiated voltage signals using a real-time spectrum analyzer. The Kolmogorov length ( $\eta \equiv \nu^{3/4}/\langle\epsilon\rangle^{1/4}$ ) and velocity ( $u_K=\nu^{1/4}\langle\epsilon\rangle^{1/4}$ ) scales were estimated using the isotropic value for the mean energy dissipation rate  $\langle\epsilon\rangle$ , i.e.,  $\langle\epsilon\rangle_{\text{iso}}=15\nu\langle(\partial u/\partial x)^2\rangle$ , with  $\langle(\partial u/\partial x)^2\rangle=\int_0^\infty k_1^2\phi_u(k_1)dk_1$ . Before carrying out this integration,  $\phi_u(k_1)$  was corrected for noise and extrapolated to large wave numbers by assuming an exponential decay of the spectrum (e.g., [17]). At the same  $y$ , there is agreement (to within 2%) between  $\langle\epsilon\rangle$  obtained from both the long and short duration data and also different probe geometries. Note that  $\langle\epsilon\rangle_{\text{iso}}$  is likely to underestimate the true value, especially near the wall [18]. Measured energy budgets from which  $\langle\epsilon\rangle$  was inferred by difference (diffusion by pressure fluctuations was neglected) confirmed this expectation. However, the use of  $\langle\epsilon\rangle_{\text{iso}}$  should be adequate for obtaining estimates of  $\eta$  and  $u_K$ ; also, the precise value of  $\langle\epsilon\rangle$  is not important in the context of this paper where the primary interest is the relative behavior of the scaling exponents.

Because of the possible errors associated with the use of Taylor's hypothesis near the wall, where the local turbulence intensity is high ( $\langle u^2\rangle^{1/2}/U>0.3$ ) and the effect of the turbulent/nonturbulent interface over the outer region, we have focused mainly on the range  $0.1\leq y/\delta\leq 0.5$ . Table I gives the Kolmogorov scales and nondimensional flow parameters  $R_\lambda$  [ $\langle u^2\rangle^{1/2}\lambda/\nu$ , where  $\lambda\equiv\langle u^2\rangle^{1/2}/\langle(\partial u/\partial x)^2\rangle^{1/2}$  is the longitudinal Taylor microscale] and mean shear  $S^*$  [ $\equiv(\partial U/\partial y)(\nu/\langle\epsilon\rangle)^{1/2}$ ] for the 200-s records within this range. Note that, over this range, the normalized mean shear is approximately constant while  $R_\lambda$  increases with  $y/\delta$ . Taylor's hypothesis is used to estimate both  $k_1$  and  $r$  from  $f$  and  $\tau$ , respectively, where  $\tau$  is a time delay. Depending on the specific context, an asterisk denotes normalization by  $\eta$ ,  $u_K$ , and/or  $\theta_K\equiv(\langle\epsilon_\theta\rangle\eta/U_K)^{1/2}$ . The temperature scale  $\theta_K$  is based on the mean temperature dissipation rate  $\langle\epsilon_\theta\rangle$  and the Kolmogorov time scale ( $\eta/U_K$ ).

## III. SPECTRAL SCALING EXPONENTS

Several different methods were used to estimate the second-order scaling exponent  $n_\beta$ . One estimate was based on identifying the optimum plateau in the compensated  $u$  spectrum. Once the widest plateau was found (by trial and

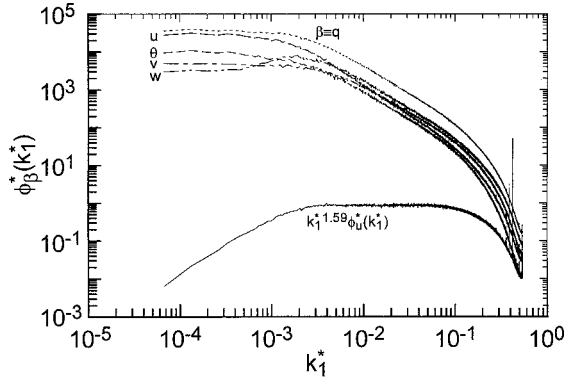


FIG. 2. Kolmogorov-normalized spectra of  $u, v, w, \theta,$  and  $q$  at  $y/\delta=0.37$ . Also shown is a compensated  $u$  spectrum to help identify the scaling range. Note that  $\int_0^\infty \phi_\beta^*(k_1^*) dk_1^* = \langle \beta^2 \rangle / U_K^2$  when  $\beta \equiv u, v, w$  and  $\langle \beta^2 \rangle / \theta_K^2$  when  $\beta \equiv \theta$ . —,  $\beta \equiv u$ ; —,  $v$ ; —,  $w$ ; —,  $\theta$ ; —,  $q$ ; —,  $k_1^{*1.59} \phi_u^*(k_1^*)$ .

error) for  $k_1^n \phi_u(k_1)$ , the exponent  $n_\beta$  ( $\beta \equiv v, w, \theta, q$ ) was subsequently inferred by least-squares fitting to  $\phi_\beta$  over the scaling range based on  $\phi_u$  [note that the exponent  $n_\beta$  is positive since it is assumed that  $\phi_\beta(k_1) \sim k_1^{-n_\beta}$  over the scaling range]. This range was also used to determine the exponent  $n_{\beta\gamma}$  corresponding to the  $\beta\gamma$  cospectrum. This approach differs somewhat from that used in [1,2] or [19] where  $n_u, n_v,$  and  $n_\theta$  were estimated by optimizing the plateau in each case. The application of this latter method to the present data would have resulted in slightly different scaling ranges for each quantity  $\beta$  and also slightly different magnitudes of  $n_\beta$ ; however, the effect on the relative magnitudes of  $n_\beta$  or its variation with  $y/\delta$  is sufficiently small not to affect the present conclusions. The scaling range in Fig. 2 ( $y/\delta = 0.37$ ;  $R_\lambda \approx 390$ ), identified by the plateau in the distribution of  $k_1^{*1.59} \phi_u^*(k_1^*)$ , is relatively large (about one decade in  $k_1^*$ ). Over this range, spectra of different quantities exhibit relatively different slopes,  $\phi_u^*$  and  $\phi_v^*$  having the largest and smallest, respectively. Note that  $\phi_w^*, \phi_q^*$ , and  $\phi_\theta^*$  have approximately the same slopes. The convention used here is that  $\int_0^\infty \phi_\beta(k_1) dk_1 = \langle \beta^2 \rangle$  while  $\int_0^\infty \phi_\beta^*(k_1^*) dk_1^* = \langle \beta^2 \rangle / U_K^2$ , when  $\beta \equiv u, v, w$  and  $\langle \beta^2 \rangle / \theta_K^2$  when  $\beta \equiv \theta$ . The distributions of  $k_1^* \phi_q(k_1^*) / \langle q^2 \rangle$  and  $k_1^* \phi_\theta(k_1^*) / \langle \theta^2 \rangle$  in Fig. 3 are nearly inseparable except at very small or very large  $k_1^*$ . This

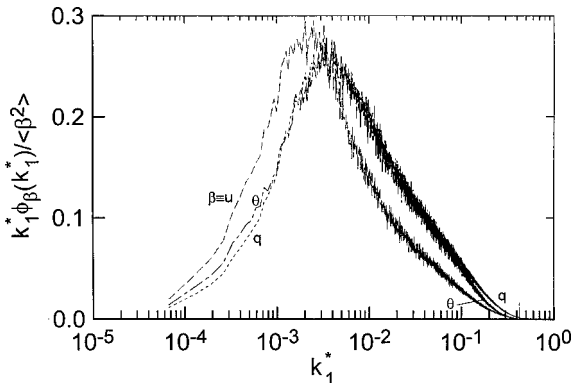


FIG. 3. Distributions of  $k_1^* \phi_\beta(k_1^*) / \langle \beta^2 \rangle$  for  $\beta \equiv u, q, \theta$  at  $y/\delta=0.37$ . Note that  $\int_0^\infty \phi_\beta(k_1^*) dk_1^* = \langle \beta^2 \rangle$ . —,  $\beta \equiv u$ ; —,  $\theta$ ; —,  $q$ .

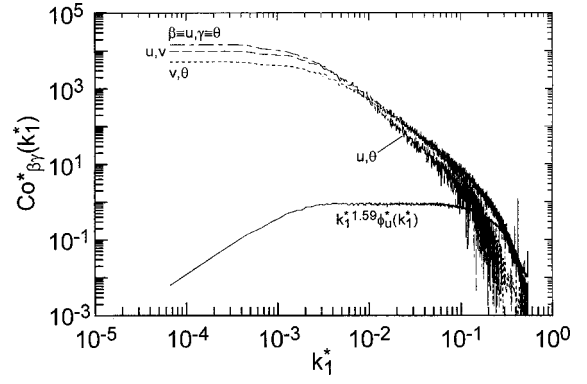


FIG. 4. Kolmogorov-normalized  $uv, u\theta,$  and  $v\theta$  cospectra at  $y/\delta=0.37$ . Also included is the same compensated  $u$  spectrum as shown in Fig. 2. —,  $\beta \equiv u, \gamma \equiv v$ ; —,  $u, \theta$ ; —,  $v, \theta$ ; —,  $k_1^{*1.59} \phi_u^*(k_1^*)$ .

closely supports the proposal of [8]; an obvious implication of the figure is that there is a significant range of turbulence length scales which contribute equally to the turbulent energy and the temperature variance. The similarity is not restricted to the most energetic scales; in this context, it is not surprising that, for the scaling range identified in Fig. 2,  $\phi_q^*(k_1^*)$  and  $\phi_\theta^*(k_1^*)$  exhibit the same slopes.

Distributions of the  $uv, u\theta,$  and  $v\theta$  cospectra measured at the same location as that for Fig. 2 are shown in Fig. 4; for reference, the compensated  $u$  spectrum of Fig. 2 is repeated here. The cospectra exhibit convincing power-law behaviors over the scaling range. The  $u\theta$  cospectrum has the largest slope (2.18) and the  $v\theta$  cospectrum the smallest (1.80); this behavior seems to reflect the relative magnitudes of the exponents  $n_u, n_\theta,$  and  $n_v$  with  $n_u$  and  $n_v$  the largest and smallest, respectively. Estimates of  $n_u, n_v, n_w,$  and  $n_\theta$ , inferred from the spectral slopes, are plotted in Fig. 5 as a function of  $y/\delta$ . Data from both short and long records are shown. All exponents decrease as the wall is approached. The greatest reduction is in  $n_v$ , whereas  $n_u$  appears to be least affected. The effect on  $n_v$  probably simply reflects the important attenuating effect the wall exerts on the  $v$  (wall-normal) fluctuation.

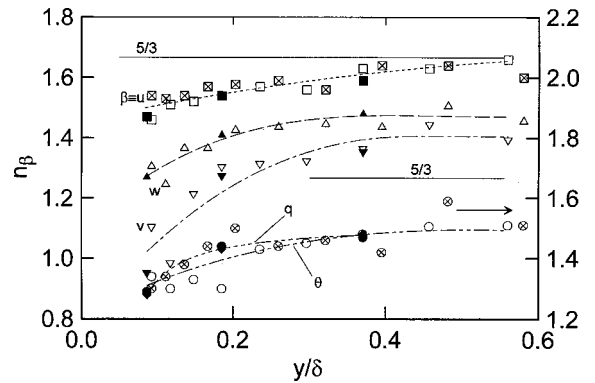


FIG. 5. Variation with  $y/\delta$  of spectral scaling exponents  $n_\beta$  for  $\beta \equiv u, v, w, q$ . Solid symbols correspond to long records; open and crossed symbols correspond to short records.  $\square, \beta \equiv u$ ;  $\nabla, v$ ;  $\Delta, w$ ;  $\circ, \theta$ ;  $\diamond, q$ . Crossed and  $\Delta$  symbols are from the  $(u, w, \theta)$  probe;  $\square, \nabla, \circ$  symbols are from the  $(u, v, \theta)$  probe. To avoid crowding,  $n_\theta$  and  $n_q$  are plotted on the right vertical axis. Lines are shown to clarify the trend for each  $n_\beta$ .

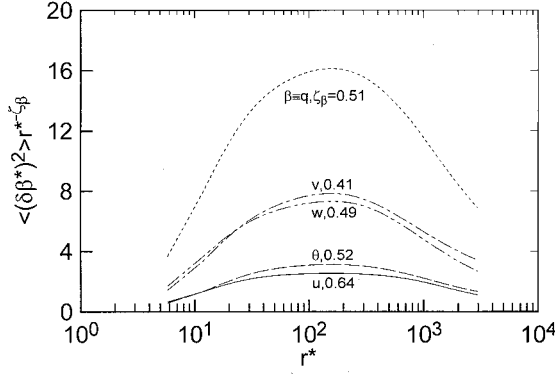


FIG. 6. Distributions of  $\langle(\delta\beta^*)^2\rangle r^{*- \zeta_\beta}$  at  $y/\delta=0.37$ . The magnitudes of  $\zeta_\beta$  are shown. —,  $\beta \equiv u$ ; — —,  $v$ ; ·····,  $w$ ; - · - ·,  $\theta$ ; ---,  $q$ .

tuation. The magnitude of  $R_\lambda$  decreases (see, e.g., Table I) as  $y/\delta$  decreases over the range of  $y/\delta$  covered here. It is tempting to ascribe the decrease in  $n_\beta$ , as  $y/\delta$  decreases, to that in  $R_\lambda$ . Such an association would be consistent, at least qualitatively, with the increase in  $n_\beta$  with  $R_\lambda$ , observed in shearless grid turbulence, or in the region straddling the axis of symmetry, for either jets or wake flows. There are, however, at least two reasons which invalidate this association. First, the present increase in  $n_v$  is larger than that measured, over an equivalent  $R_\lambda$  range, in the previously mentioned flows or flow regions. Second, as mentioned in Sec. I,  $n_u$  (and *a fortiori*  $n_v$ ) also decreases as a smooth wall is approached. For the channel flow investigation of [13],  $n_u$  was found to decrease continuously between the center line and  $y^+ \approx 20$  (a similar trend was reported by [14]); and yet,  $R_\lambda$  increases from the center line to a maximum near  $y^+ \approx 10$  [20]. This trend is opposite to that observed over the present rough wall. A more likely explanation for the decrease in  $n_\beta$  close to the wall is that suggested in [13–15]. That is, there is an increased intermittency of the energy dissipation rate due to the presence of relatively intense vortical structures near the wall. The vortical structures near the present rough wall are likely to differ, with respect to both geometry, intensity, and also frequency of occurrence from those over a smooth wall or indeed over a different type of surface roughness. Some evidence for this was given in [21]. A consequence of the previous speculation is that each type of surface will have its own distribution of  $n_\beta$ .

#### IV. SCALING EXPONENTS FROM STRUCTURE FUNCTIONS

A second method of estimating a scaling exponent, closely related to that described in Sec. III, is to determine the “best” power-law exponents for the second-order structure functions  $\langle(\delta\beta)^2\rangle$ , having first identified the scaling range. For consistency with the first method, this range is that corresponding to the widest plateau in  $\langle(\delta u)^2\rangle r^{-\zeta_u}$  which also compares well with the plateau in  $\langle(\delta u)^3\rangle r^{-1}$ . The exponents  $\zeta_\beta$  ( $\beta \equiv v, w, \theta, q$ ) and  $\zeta_{\beta\gamma}$  ( $\beta \equiv u, \gamma \equiv v; u, \theta; v, \theta$ ) were subsequently obtained by applying least-

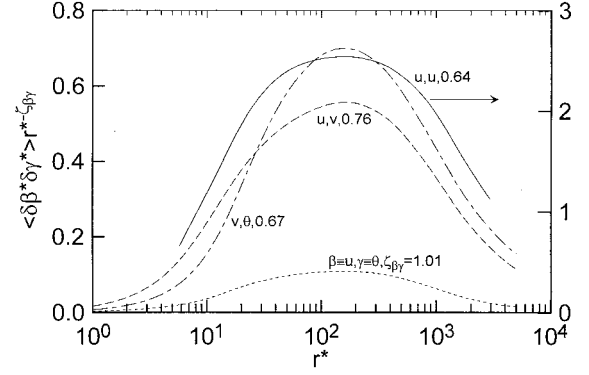


FIG. 7. Distributions of  $\langle\delta\beta^* \delta\gamma^*\rangle r^{*- \zeta}$  at  $y/\delta=0.37$ . The magnitudes of  $\zeta_{\beta\gamma}$  are shown. —,  $\beta \equiv u, \gamma \equiv u$ ; - - -,  $u, v$ ; ·····,  $u, \theta$ ; - · - ·,  $v, \theta$ .

squares fits to  $\langle(\delta\beta)^2\rangle$  and  $\langle(\delta\beta)(\delta\gamma)\rangle$  over the scaling range.

The corresponding distributions of  $\langle(\delta\beta^*)^2\rangle r^{*- \zeta_\beta}$  and  $\langle(\delta\beta^*)(\delta\gamma^*)\rangle r^{*- \zeta_{\beta\gamma}}$  are shown in Fig. 6 and 7, respectively. The plateau in  $\langle(\delta u^*)^2\rangle r^{*- \zeta_u}$  is not as wide as that exhibited by  $k_1^{*n_u} \phi_u^*(k_1^*)$  implying scaling ranges of different extents. A similar observation was made by [22]. Note also that the values of  $n_u (=1.59)$  and  $\zeta_u (=0.64)$  do not quite correspond in that  $n_u$  is smaller than  $(1 + \zeta_u)$ . This correspondence has been discussed in some detail by Hou *et al.* [23], who emphasized that the finiteness of the power-law range makes the translation between the power law of the spectrum and that of either the correlation function or structure function inexact. Not surprisingly, the validity of this translation improves as  $R_\lambda$  increases (e.g., [24]) and the power-law range dilates.

Notwithstanding the inexactness of the translation for the present moderate values of  $R_\lambda$ , the relative magnitudes of different  $\zeta_\beta$  and their variation with  $y/\delta$  (Fig. 8) are closely similar to those of  $n_\beta$  in Fig. 5. In particular, the rate of increase of  $\zeta_u$  with  $y/\delta$  is relatively small while that of  $\zeta_v$  is largest.

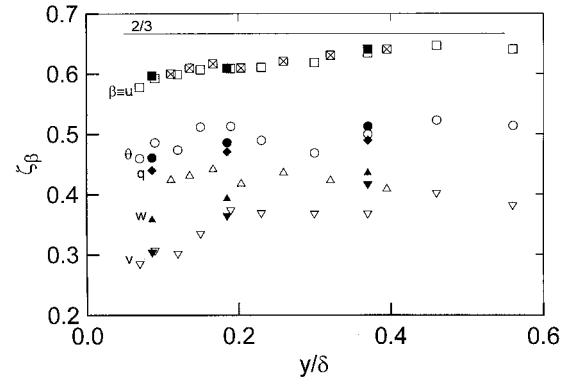


FIG. 8. Variation with  $y/\delta$  of scaling range exponents  $\zeta_\beta$  for  $\beta \equiv u, v, w, \theta, q$  obtained for the same scaling range as was determined using  $\langle(\delta u^*)^2\rangle r^{-\zeta_u}$ . Solid symbols correspond to long records; open and crossed symbols correspond to short records. □,  $\beta \equiv u$ ; ▽,  $v$ ; △,  $w$ ; ○,  $\theta$ ; ◇,  $q$ . ⊠ and ⊞ symbols are from the  $(u, w, \theta)$  probe; □, ▽, ○ symbols are from the  $(u, v, \theta)$  probe.

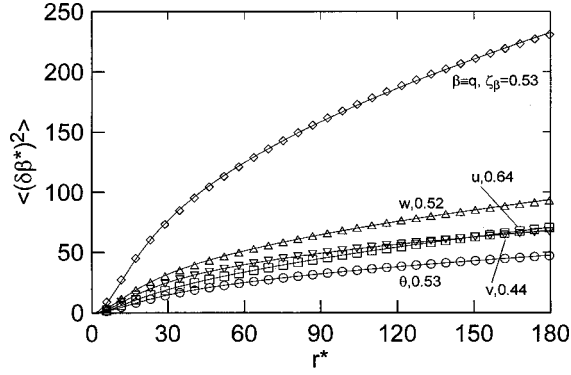


FIG. 9. Kolmogorov-normalized structure functions of  $u$ ,  $v$ ,  $w$ ,  $\theta$ , and  $q$  at  $y/\delta=0.37$ . Solid lines are fits to the measurements obtained with Eq. (1). The magnitudes of  $\zeta_\beta$  are shown.  $\square$ ,  $\beta \equiv u$ ;  $\nabla$ ,  $v$ ;  $\triangle$ ,  $w$ ;  $\circ$ ,  $\theta$ ;  $\diamond$ ,  $q$ .

Two other estimations of  $\zeta_\beta$  have been carried out. The first uses the relation

$$\langle(\delta\beta^*)^2\rangle = \frac{a_\beta r^{*2}}{[1 + b_\beta r^{*2}]^{c_\beta}}, \quad (1)$$

as a relatively reliable descriptor of the behavior of  $\langle(\delta\beta^*)^2\rangle$  for values of  $r^*$  which span the dissipative range and a significant portion of the inertial range. Equation (1) has been used by a number of authors (e.g., [25]) with  $\beta \equiv u$ . It has also been applied to data for  $\beta \equiv u, v$ , or  $\theta$  [26,27] to determine the  $R_\lambda$  dependence of  $c_\beta \equiv (2 - \zeta_\beta)/2$  in several flows (grid turbulence, jets, and wakes). Figure 9 indicates that Eq. (1) fits the measured distributions of  $\langle(\delta\beta^*)^2\rangle$  quite well. There is some arbitrariness [26] associated with the selection of  $r_{\max}^*$ , the maximum value of  $r^*$  used for fitting to the data. The magnitude of  $\zeta_\beta$  is relatively insensitive to the choice of  $r_{\max}^*$ , where a significant plateau is observed in Fig. 6; indeed, a similar maximum is obtained using  $\langle(\delta u^*)^3\rangle r^{*-1}$  (not shown). The uncertainty in determining  $\zeta_\beta$  increases when  $R_\lambda$  is small and the plateau is absent. The relative values of  $\zeta_\beta$ , indicated on each curve (Fig. 9), closely mimic those of  $n_\beta$  inferred from the spectra (Fig. 5) and are in close agreement with those of  $\zeta_\beta$  shown in Fig. 8. In particular,  $\zeta_v$  is smallest and  $\zeta_u$  largest;  $\zeta_q$  and  $\zeta_\theta$  have the same magnitude. Whereas the distributions of  $\langle(\delta q^*)^2\rangle$  and  $\langle(\delta\theta^*)^2\rangle$  are different, the distributions of  $\langle(\delta q)^2\rangle/\langle q^2\rangle$  and  $\langle(\delta\theta)^2\rangle/\langle\theta^2\rangle$  (Fig. 10) follow each other closely.

Significant use has been made of the extended self-similarity (ESS) method [28] for determining  $\zeta_\beta$ . This method is less effective when it is applied in regions where the effect of the mean shear is significant [29]; for this reason, ESS estimates of  $\zeta_\beta$  are not presented.

## V. INTERMITTENCY EXPONENTS

An estimate of the intermittency parameters  $\mu_\beta$ , associated with each of the main quantities, was determined from the scaling exponents  $\zeta_\beta(2,4)$ , where

$$\langle(\delta u)^2(\delta\beta)^4\rangle \sim r^{\zeta_\beta(2,4)}$$

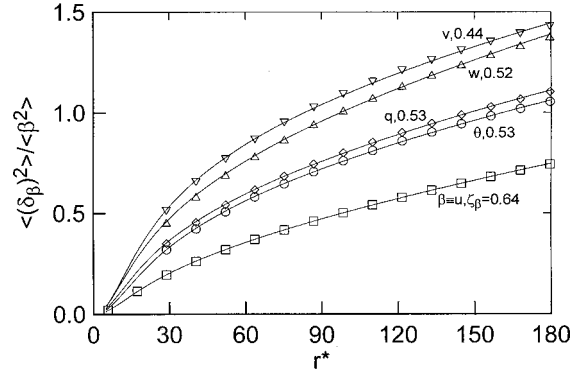


FIG. 10. Distributions of  $\langle(\delta\beta)^2\rangle$  normalized by the variance  $\langle\beta^2\rangle$  at  $y/\delta=0.37$ . Solid lines are fits to the measurements obtained with the nondimensional form of Eq. (1). The magnitudes of  $\zeta_\beta$  are shown.  $\square$ ,  $\beta \equiv u$ ;  $\nabla$ ,  $v$ ;  $\triangle$ ,  $w$ ;  $\circ$ ,  $\theta$ ;  $\diamond$ ,  $q$ .

( $\beta \equiv u, v, w, \theta, q$ ) via the relation

$$\mu_\beta = 2 - \zeta_\beta(2,4). \quad (2)$$

To determine  $\mu_q$ ,  $\langle(\delta u)^2(\delta q)^4\rangle$  was approximated by the expression  $\{ \langle(\delta u)^6\rangle + 2[\langle(\delta u)^2(\delta v)^4\rangle + \langle(\delta u)^2(\delta w)^4\rangle + \langle(\delta u)^4(\delta v)^2\rangle + \langle(\delta u)^4(\delta w)^2\rangle] \}$  since the term  $\langle(\delta u)^2(\delta v)^2(\delta w)^2\rangle$  was not measured. Figure 11 shows the variation of  $\mu_\beta$  with  $y/\delta$ ; only the longer records were used in order to minimize the uncertainty of estimating mixed sixth-order moments. As the distance from the wall increases, the magnitude of  $\mu_\beta$  decreases. This is not consistent with the concomitant increase in  $R_\lambda$  but it is consistent with the previously reported increase in  $n_\beta$  (or  $\zeta_\beta$ ) with  $y/\delta$ . The magnitude of  $\mu_u$  at  $y/\delta=0.37$  is significantly larger than that for the high  $R_\lambda$  atmospheric flow of [30] or the cocensus value ( $\approx 0.25$ ) suggested in [31]. The difference between the present intermittency exponents and those usually quoted for “fully developed” turbulence, under nearly homogeneous and isotropic conditions, is not surprising. One expects the spatial intermittency of both the velocity and temperature dissipation rates to increase as the wall is approached and the effect of the shear, presumably via the relatively intense near-wall vortical structures, becomes more pronounced. It is

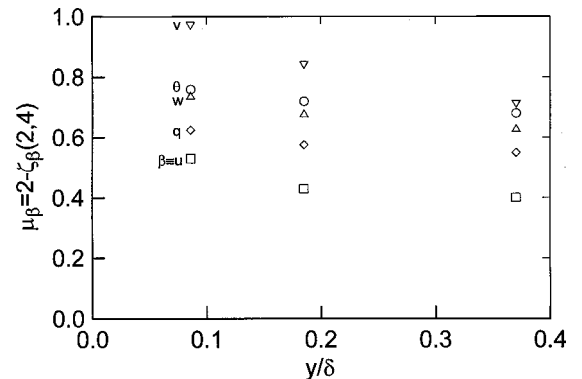


FIG. 11. Variation with  $y/\delta$  of intermittency parameters  $\mu_\beta$  for  $\beta \equiv u, v, w, \theta, q$ . Only data from the longer records have been used.  $\square$ ,  $\beta \equiv u$ ;  $\nabla$ ,  $v$ ;  $\triangle$ ,  $w$ ;  $\circ$ ,  $\theta$ ;  $\diamond$ ,  $q$ .

also reasonable that the magnitude of  $\mu_v$  is larger than that of  $\mu_u$  or  $\mu_w$  given that  $v$  is most affected by the presence of the wall. The larger value of  $\mu_\theta$ , relative to  $\mu_u$ , is also not surprising but the small difference between the magnitudes of  $\mu_\theta$  and  $\mu_q$  contrasts somewhat with the near-equality between  $\zeta_\theta$  (or  $n_\theta$ ) and  $\zeta_q$  (or  $n_q$ ). A possible cause for this may be the approximation we have used to generate  $\langle(\delta u)^2(\delta q)^4\rangle$ . A more likely possibility is the nonperfect correlation that exists between  $\epsilon$  and  $\epsilon_\theta$ . This will be the subject of a future investigation.

The present  $\mu_\beta$  estimates, via Eq. (2), have been obtained independently from intermittency models. It is therefore of interest to see how the models compare with the data for  $\langle(\delta\beta)^2\rangle$ , when the present estimates of  $\mu_\beta$  are used. The log-normal [7] and She-L ev eque [32] models both indicate that the magnitude of  $\zeta_u$  exceeds  $\frac{2}{3}$  and increases with increasing  $\mu_u$ . In contrast, Fig. 5 indicates that  $\zeta_u$  is always smaller than  $\frac{2}{3}$ . The log-normal model for temperature [33] predicts that the magnitude of  $\zeta_\theta$  is smaller than  $\frac{2}{3}$ . While this result is in qualitative agreement with  $\zeta_\theta$  in Fig. 5, the measured values of  $\zeta_\theta$  are significantly smaller than those predicted. Also, the decrease of  $\zeta_\theta$  with decreasing  $y$  is not reproduced by the model which indicates an increase in  $\zeta_\theta$  as  $\mu_\theta$  increases. The discrepancy between the predictions and the measurements is not surprising since the models were developed for high Reynolds number, homogeneous, and isotropic turbulence.

## VI. CONCLUSIONS

Power-law exponents, associated with the scaling range, are estimated for both spectra and structure functions of several quantities, including all three velocity fluctuations and the temperature fluctuation measured in a turbulent boundary layer over a rough wall. These estimates, obtained using a number of different methods, are in quite reasonable agreement with each other. For each method, the magnitudes of the exponents decrease as the wall is approached. The reduction is ascribed to the increased intermittency due to the relatively intense near-wall vortical structures. The greatest reduction is observed for the exponents  $n_v$  and  $\zeta_v$  associated with  $\phi_v$  and  $\langle(\delta v)^2\rangle$ , respectively. Consistently, the intermittency exponent  $\mu_v$  is greater than either  $\mu_u$ ,  $\mu_w$ , or  $\mu_\theta$ . The magnitudes of  $n_q$  and  $\zeta_q$ , the scaling exponents corresponding to  $\phi_q$  and  $\langle(\delta q)^2\rangle$ , respectively, are in close agreement with those of  $n_\theta$  and  $\zeta_\theta$ . This agreement supports the role played by the fluctuating velocity vector in advecting the passive scalar, especially in the present flow where the presence of the roughness is expected to result in an enhanced mixing of the scalar.

## ACKNOWLEDGMENTS

We are grateful for the support of the Australian Research Council and to Professor P.- . Krogstad for assistance with the experimental design and data acquisition.

- 
- [1] K. R. Sreenivasan, Proc. R. Soc. London, Ser. A **434**, 165 (1991).
- [2] K. R. Sreenivasan, Phys. Fluids **8**, 189 (1996).
- [3] A. N. Kolmogorov, Dokl. Akad. Nauk SSSR **30**, 301 (1941).
- [4] B. Dhruva, Y. Tsuji, and K. R. Sreenivasan, Phys. Rev. E **56**, R4928 (1997).
- [5] B. R. Pearson, Ph.D. thesis, University of Newcastle, 1999 (unpublished).
- [6] B. R. Pearson and R. A. Antonia (unpublished).
- [7] A. N. Kolmogorov, J. Fluid Mech. **13**, 82 (1962).
- [8] L. Fulachier and R. Dumas, J. Fluid Mech. **77**, 257 (1976); L. Fulachier and R. A. Antonia, Int. J. Heat Mass Transf. **27**, 987 (1984).
- [9] R. A. Antonia, Y. Zhu, F. Anselmet, and M. Ould-Rouis, Phys. Fluids **8**, 3105 (1996).
- [10] R. A. Antonia and B. R. Pearson, Europhys. Lett. **40**, 123 (1997); B. R. Pearson, T. Zhou, and R. A. Antonia, *ibid.* **44**, 156 (1998).
- [11] P. Mestayer, J. Fluid Mech. **125**, 475 (1982).
- [12] A. M. Obukhov, Izv. Akad. Nauk SSSR, Ser. Geogr. Geofiz. **13**, 58 (1949); S. Corrsin, J. Appl. Phys. **22**, 469 (1951).
- [13] R. A. Antonia, P. Orlandi, and G. P. Romano, Phys. Fluids **10**, 3239 (1998).
- [14] G. Amati, S. Succi, and R. Piva, Fluid Dyn. Res. **24**, 201 (1999).
- [15] F. Toschi, G. Amati, S. Succi, R. Benzi, and R. Piva, Phys. Rev. Lett. **82**, 5044 (1999).
- [16] P.- . Krogstad, R. A. Antonia, and L. W. B. Browne, J. Fluid Mech. **245**, 599 (1992).
- [17] D. O. Martinez, S. Chen, G. D. Doolen, R. H. Kraichnan, L. P. Wang, and Y. Zhou, J. Plasma Phys. **57**, 195 (1997).
- [18] R. J. Smalley, P.- . Krogstad, and R. A. Antonia, in *Proceedings of the Thirteenth Australasian Fluid Mechanics Conference, Melbourne, 1998*, edited by M. C. Thompson and K. Hourigan (Monash University Press, Melbourne, 1998), p. 615.
- [19] L. Mydlarski and Z. Warhaft, J. Fluid Mech. **320**, 331 (1996); **358**, 135 (1998).
- [20] R. A. Antonia, J. Kim, and L. W. B. Browne, J. Fluid Mech. **233**, 369 (1991).
- [21] P.- . Krogstad and R. A. Antonia, J. Fluid Mech. **277**, 1 (1994).
- [22] B. R. Pearson and R. A. Antonia, in *Proceedings of the Eighth Asian Congress of Fluid Mechanics, Shenzhen, 1999*, edited by E. Cui (International Academic Publishers, Beijing, 1999), p. 145.
- [23] T. Y. Hou, X.-H. Wu, X. Chen, and Y. Zhou, Phys. Rev. E **58**, 5841 (1998).
- [24] A. S. Monin and A. M. Yaglom, *Statistical Fluid Mechanics* (MIT Press, Cambridge, MA, 1975); T. D. Dickey and G. L. Mellor, Phys. Fluids **22**, 1029 (1979).
- [25] G. Stolovitzky, K. R. Sreenivasan, and A. Juneja, Phys. Rev. E **48**, R3217 (1993); S. Grossmann, *ibid.* **51**, 6275 (1995); G. Stolovitzky and K. R. Sreenivasan, *ibid.* **52**, 3242 (1995); C. Meneveau, *ibid.* **54**, 3657 (1996).
- [26] R. A. Antonia, B. R. Pearson, and T. Zhou (unpublished).
- [27] R. A. Antonia, T. Zhou, and G. Xu, Phys. Fluids **12**, 1509 (2000).
- [28] R. Benzi, S. Ciliberto, R. Tripiccone, C. Baudet, F. Massaioli, and S. Succi, Phys. Rev. E **48**, R29 (1993).
- [29] R. Benzi, L. Biferale, S. Ciliberto, M. V. Struglia, and R. Tri-

- piccione, *Europhys. Lett.* **32**, 709 (1995).
- [30] A. J. Chambers and R. A. Antonia, *Boundary-Layer Meteorol.* **28**, 343 (1984).
- [31] K. R. Sreenivasan and P. Kailasnath, *Phys. Fluids A* **5**, 412 (1993).
- [32] Z. S. She and E. Lévéque, *Phys. Rev. Lett.* **72**, 336 (1994).
- [33] N. N. Korchashkin, *Izv., Acad. Sci., USSR, Atmos. Oceanic Phys.* **6**, 947 (1970).